Biosensors and Bioelectronics 183 (2021) 113243

Contents lists available at ScienceDirect

Biosensors and Bioelectronics

journal homepage: http://www.elsevier.com/locate/bios

MXene-based enzymatic sensor for highly sensitive and selective detection of cholesterol

Tianzi Xia [a], Guangyan Liu [a], Junjie Wang [a], Shili Hou [a,*], Shifeng Hou [a,b,**]

[a] Guangxi Key Laboratory of Electrochemical and Magneto-chemical Functional Materials, College of Chemistry and Bioengineering, Guilin University of Technology, Guangxi, 541006, PR China

[b] National Engineering and Technology Research Center for Colloidal Materials, Shandong University, Jinan, Shandong, 250100, PR China

ARTICLE INFO

Keywords:
MXene
Biosensor
Cholesterol oxidase
Cholesterol

ABSTRACT

In this work, the synthesized MXene ($Ti_3C_2T_x$) exhibited large specific area, biocompatibility, excellent electronic conductivity, and good dispersion in aqueous phase. The Chit/ChOx/$Ti_3C_2T_x$ nanocomposite was prepared through the continuous self-assembled process. Its structure is characterized by scanning electron microscopy (SEM), cyclic voltammetry (CV), electrochemical impedance spectroscopy (EIS), and differential pulse voltammetry (DPV). Moreover, the biosensor for cholesterol detection was fabricated via a one-step dip-coating method. Chit and$Ti_3C_2T_x$ act as a support matrix to immobilize ChOx enzyme, and also play a role in increasing the electrical conductivity. Meanwhile, the addition of redox mediator ($Fe(CN)_6^{3-/4-}$) facilitates the electron transport from the analyte to the modified electrode in the oxidation of cholesterol. The DPV response exhibited an increase in current with increasing cholesterol concentration. Under the optimum conditions, the DPV response of the biosensor indicated a good linear relationship with the concentration of cholesterol ranging from 0.3 to 4.5 nM with a low detection limit of 0.11 nM, and a high sensitivity of 132.66 μA nM^{-1} cm^{-2}. In addition, with favorable selectivity and stability, the biosensor has been used to detect cholesterol in real samples and the results demonstrate that the biosensor has excellent practicability.

1. Introduction

Cholesterol as a significant lipid in human beings, a waxy steroid present in fats, is a major part of cell membrane and helps to maintain membrane permeability and fluidity. At the same time, cholesterol is an important biomarker for a number of diseases (Devadoss and Burgess, 2004). The low content of cholesterol may cause several diseases such as low lipoprotein, sepsis, malnutrition, anemia (Huang et al., 2019). While the high content of cholesterol may be associated with a variety of diseases, such as hypertension, cerebral thrombosis, coronary heart disease, and atherosclerosis (Sekretaryova et al., 2014). In general, 2.83 – 5.20 mM is the normal range of human cholesterol level to be maintained (Amiri and Arshi, 2020). Hence, the development of a simple, precise, sensitive, and effective method for monitoring cholesterol concentration is important practical significance in academic and medical fields.

To date, high performance liquid chromatography (Sinha et al., 2015), colorimetry (Zhao et al., 2019), fluorescence (Sun et al., 2017), spectrophotometry (Chitra et al., 2017), electrochemiluminescence (Wu et al., 2014) and electrochemistry (Yuan, 2013; Maduraiveeran et al., 2018) have been used for the detection of cholesterol. Most of these methods have good results in cholesterol detection, but some shortcomings still exist in the case of time consumption, low sensitivity, and selectivity, sophisticated instrumentation standardization difficulties, requirement of sample pretreatment and experienced operators (Amiri and Arshi, 2020). However, electrochemical biosensor approach overcomes these disadvantages, which are highly specific, simplicity, cost-effective, and highly sensitive (Narwal et al., 2019). For example, Zandi et al. (2019) reported the electrochemical lipidomics based on electrical impedance spectroscopy (EIS) to detect carcinoma in secretory glands. This technique may provide new insights into cancer diagnosis as a cell free complementary analysis. Nandini et al. (2016) had constructed a sensitive biosensor, AuNs/SHGO/ChOx/Graphit, to analyze the cholesterol with a low limit of detection (LOD) of 0.2 nM. To this

* Corresponding author.
** Corresponding author. Guangxi Key Laboratory of Electrochemical and Magneto-chemical Functional Materials, College of Chemistry and Bioengineering, Guilin University of Technology, Guangxi, 541006, PR China.
E-mail addresses: houshili@glut.edu.cn (S. Hou), shifenghou@sdu.edu.cn (S. Hou).

https://doi.org/10.1016/j.bios.2021.113243
Received 1 March 2021; Received in revised form 5 April 2021; Accepted 7 April 2021
Available online 15 April 2021

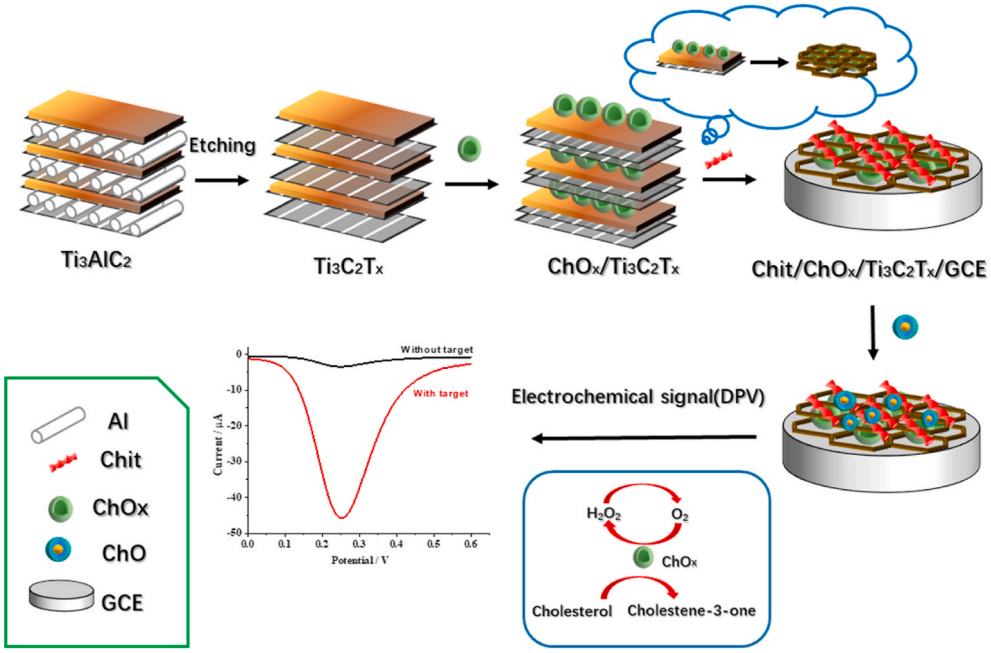

Fig. 1. A schematic representation of the fabrication of the Chit/ChOx/$Ti_3C_2T_x$/GCE, and a possible reaction mechanism of cholesterol at the modified GCE.

end, enzymes have been immobilized on electrodes with different carriers based on nanomaterials, polymers, hydrogels and sol-gels, self--assembly monolayers, and other materials (Amiri and Arshi, 2020). The sensing nanomaterials play an important role in the enhanced sensitivity of biosensors. Until now, because of carbon nanomaterials' large specific surface areas, good biocompatibility, and excellent electrical conductivity, they have been widely used as sensing materials for immobilizing enzymes and fabricating biosensors (Alwarappan et al., 2010a, 2010b, 2012; Huo et al., 2016; Wan et al., 2015). In addition, semiconductor metal oxides, MoO_3 with a unique layered structure is promising candidate materials for sensors (Yang et al., 2016). It is well known that the uniform dispersion of nanomaterials in water solution is the key to promote their application in enzymatic biosensors (Malig et al., 2012). Nevertheless, carbon nanomaterials are difficult to disperse uniformly in aqueous phase, due to their hydrophobic nature.

Recently, transition metal carbides, nitrides, and carbonitrides (MXene) have been introduced into the field of electrochemical biosensor due to their outstanding metal conductivity, hydrophilic surface, large specific surface area, layered structure, remarkable chemical stability, and rich surface chemical groups (Zhang et al., 2020; Soomro et al., 2020; Kalambate et al., 2019; Liu et al., 2019). MXene is a novel class of two-dimensional materials of transition metal carbides, and nitrides (Naguib et al., 2011). MXene can be obtained by etching element A from the raw material MAX powders, where M generally stands for an early transition metal, A is mostly IIIA or IVA of a periodic table element, and X represents carbon or nitrogen. And that MXene general formula is $M_{n+1}X_nT_x$, T_x stands for surface functional groups (-O, –OH, –F), M and X are the same as above. MXene has great application prospects in supercapacitor (Yu et al., 2018), catalysts (Seh et al., 2016), electromagnetic shielding (Urbankowski et al., 2017) and lithium-sulfur batteries (Ma et al., 2020). Because of the large surface, the MXene-based materials are comparable and superior to some other two-dimensional materials in immobilizing enzymes or proteins to achieve accelerated reaction kinetics. However, the 2D materials containing MXene are easy to agglomerate or stacked in nature hindering the ion transmission by the electrodes. In order to make full use of the electrochemical performance of MXene, a number of methods have been developed to create porous structures or introduce interlayer spacers into MXene. Thus, it is increasingly reported that the construction of 2D materials into 3D macroscopic structures, such as films or aerogels, which can greatly accelerate ion transport in electrodes for efficient devices (Yao et al., 2021). In addition, chitosan (Chit) is widely used as a biomaterial for immobilizing enzymes. It exhibits excellent film-forming ability, biocompatibility, nontoxicity, high mechanical strength, and hydrophilicity for constructing electrochemical biosensors (Farshchi et al., 2020). So far, MXene-Ti_3C_2 immobilized hemoglobin and tyrosinase has been used to the detection of $NaNO_2$ and phenol with the LOD of 0.12 μM and 12 nM, respectively (Liu et al., 2015; Wu et al., 2018). And MXene-Ti_3C_2 combined with TiO_2 nanoparticles immobilized hemoglobin exhibited LOD of 14 nM for H_2O_2 with good performances (Wang et al., 2015). MXene-based enzymatic biosensors have been developed rapidly, due to their fast response, high sensitivity, good inherent selectivity, and biocompatibility. However, because of enzymatic deactivation, high cost and difficulty in preparation, their widespread applications have been restricted. To data, few studies on enzymatic biosensors based on MXene have been reported (Sajid, 2021). Hence, in view of MXene's unique structure and excellent properties, its application in immobilizing enzyme and fabricating biosensor is worthy of further study.

In this study, we fabricated a sensitive and simple MXene-based enzymatic electrochemical biosensor, which was constructed by utilizing the beneficial properties of MXene and Chit. Herein, this biosensor began with the hierarchical etching of Ti_3AlC_2 to form $Ti_3C_2T_x$ as a template for immobilizing cholesterol oxidase (ChOx), following, the continuous self-assembled process was designed to form the hierarchical accordion-like Chit/ChOx/$Ti_3C_2T_x$ nanocomposite. Chit and $Ti_3C_2T_x$ help to immobilize ChOx, and also play a role in conducting media for electron transfer. Moreover, its electrochemical behaviors were studied by differential pulse voltammetry (DPV). The DPV response of determination of cholesterol is generated via the ChOx reaction, which is selective oxidation of cholesterol to cholest-4-en-3-one and H_2O_2. With the production of H_2O_2, the electro-oxidation current can be detected at the appropriate potential. It can measure the level of cholesterol indirectly. Meanwhile, the addition of redox mediator ($Fe(CN)_6^{3-/4-}$) facilitates the electron transport from the analyte to the modified electrode. Thus, the redox mediator plays a significant role in the oxidation of cholesterol and the fast reversible electron transfer accelerates the kinetics of the electrochemical reaction (Fig. 1). Satisfactorily, it is

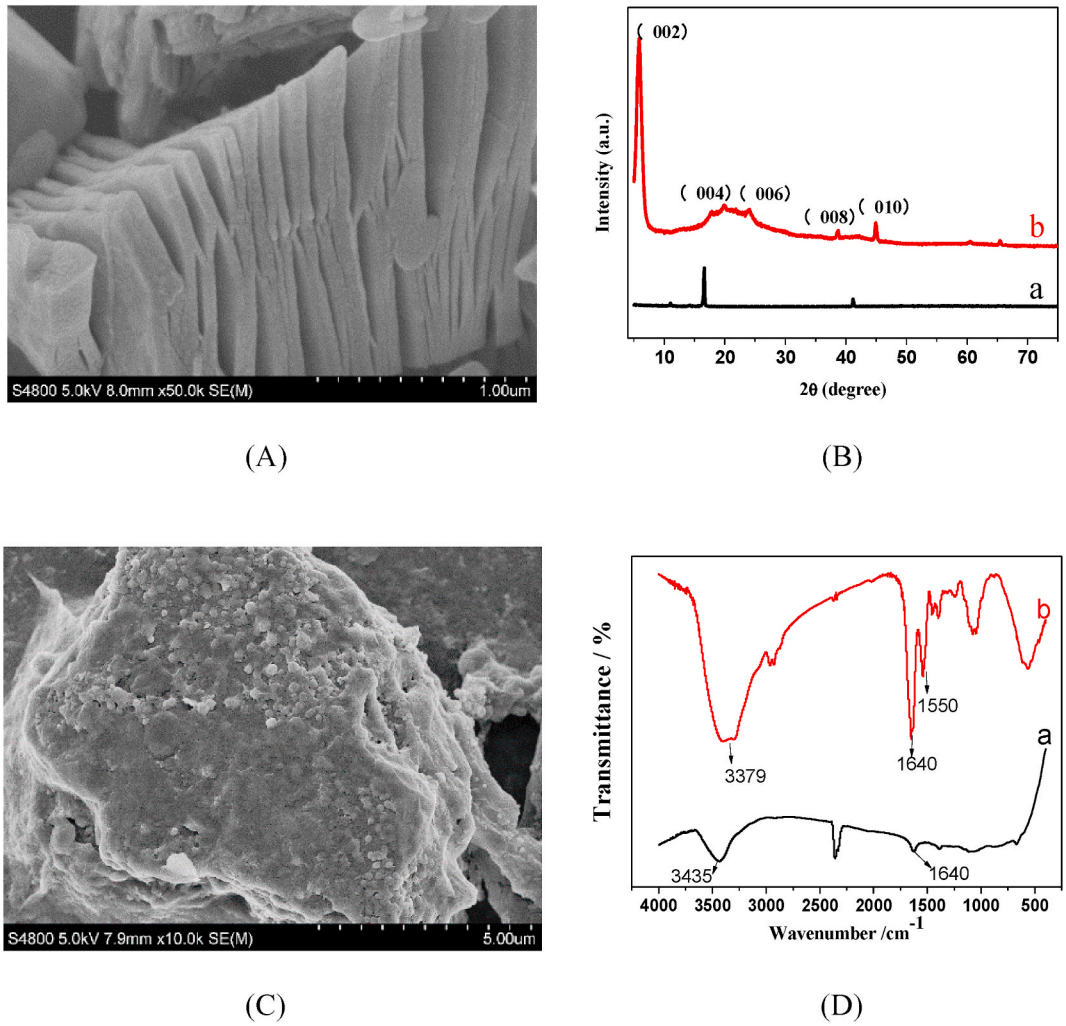

Fig. 2. (A) SEM of MXene. (B) XRD of Ti_3AlC_2 (a) and $Ti_3C_2T_x$ (b). (C) SEM images of MXene/Chit/ChOx/film on GCE. (D) IR spectra of $Ti_3C_2T_x$ (a) and ChOx/$Ti_3C_2T_x$ (b).

demonstrated to be a successful electrochemical biosensor with a good linear response and low detection limit, exhibiting excellent performance for the determination of cholesterol concentration. Furthermore, the proposed electrochemical method has been successfully applied for the detection of cholesterol in real samples with excellent stability and reproducibility.

2. Experimental section

2.1. Materials

Ti_3AlC_2 powder (300 mesh) was purchased from 11 Technology Co., Ltd (Jilin, China). Chitosan (Chit, from shrimp shells, ≥ 95% deacetylated), cholesterol (Cho, > 99%), cholesterol oxidase (ChOx, >10 U mg^{-1}), and bovine serum albumin (BSA, ≥ 98%) were purchased from Aladdin (Shanghai, China). Hydrochloric acid (HCl, 37%), lithium fluoride (LiF), Triton X-100, isopropyl alcohol (IPA), potassium chloride (KCl), $K_3[Fe(CN)_6]$, $K_4[Fe(CN_6)]$, glucose (Glu), lactic acid (LA), uric acid (UA) and other reagents were purchased from local chemical reagent company. Unless otherwise noted, all reagents were analytical grade. Chit was prepared in 0.1 M acetic acid, 0.1 M phosphate buffer solution (PBS, pH 7.0) obtained NaH_2PO_4 and Na_2HPO_4 were used as supporting electrolytes. PBS solution of different pH was adjusted by NaH_2PO_4 and Na_2HPO_4. Ultrapure water (resistance: 18.25 MΩ $cm^{-1)}$ was used for the preparation of all the solutions. Stock solutions of ChOx were in PBS solution. The stock solution of Cholesterol was obtained by dissolving cholesterol in a mixture solution of Triton X-100 (1.5 mL), isopropanol (1.5 mL), and PBS (17 mL) under magnetic stirring at a temperature of 60 °C to preparation a standard solution. The standard solution was diluted to create different concentrations of analytes by PBS (pH 7.0) for further experimentation. The human serum sample was collected from the Affiliated Hospital of Guilin University of Technology, and diluted to 50-fold using PBS (0.1 M pH 7.0).

All reagents were used in this paper and without further purification. The prepared stock solution was stored at 4 °C before use.

2.2. Apparatus

The electrochemical measurements were performed on a CHI 660E (Shanghai Chenhua Instrument, China) electrochemical workstation. Electrochemical impedance spectroscopy (EIS) was performed on an Autolab workstation (Eco Chemie, Utrecht, Netherlands). All electrochemical experiments were carried out using a three-electrode system with a glassy carbon electrode (GCE diameter of 3 mm) as the working electrode, an Ag/AgCl as the reference electrode, and a platinum wire electrode as the auxiliary electrode. Fourier transform infrared spectroscopy (FT-IR) assay was obtained a Nicolet iS10 Fourier IR Spectrometer (Thermo Fisher Scientific, USA). Scanning electron microscope (SEM) was JSM-7610 F (JEOL Ltd., Japan) carried out on morphologies. X-ray diffraction (XRD) study was performed using an X'pert PRO

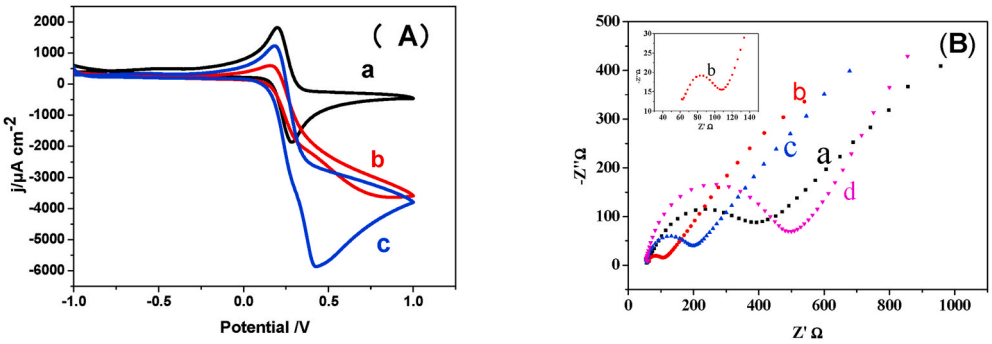

Fig. 3. (A) CVs of bare GCE (a), Chit/ChOx/GCE (b) Chit/ChOx/$Ti_3C_2T_x$/GCE (c) in 1 mM $Fe(CN)_6^{3-/4-}$ solution containing 0.1 M KCl and 1.0 mM cholesterol. Scan rate: 100 mV s^{-1}. (B) Nyquist plots of Chit/ChOx/$Ti_3C_2T_x$/GCE (a), $Ti_3C_2T_x$/GCE (b), GCE (c), Chit/ChOx/GCE (d) in 1 mM $Fe(CN)_6^{3-/4-}$ containing 0.1 M KCl and 1.0 mM cholesterol. Inset: Amplified Nyquist plot of (b) $Ti_3C_2T_x$/GCE.

powder diffractometer (Netherlands). All measurements were conducted at 25 °C.

2.3. Synthesis of MXene nanosheets ($Ti_3C_2T_x$)

The MXene-$Ti_3C_2T_x$ were synthesized according to the literature with a little modification (Urbankowski et al., 2017). Typically, LiF powder (1.0 g) was dissolved in 20 mL of 9 M HCl solution. After 1.0 g of Ti_3AlC_2 was slowly added into the above solution. The mixture was constant magnetic stirred at 40 °C for 30 h. The resulting suspension was washed with ultrapure water for five times and centrifuged at 3500 rpm for 10 min, then washed with ultrapure water until the pH of the supernatant was close to 6. Following, the stable $Ti_3C_2T_x$ suspension was subjected to sonication for 1 h. Finally, the obtained $Ti_3C_2T_x$ were dried in a vacuum at 60 °C for 15 h.

2.4. Preparation of chit/ChOx/$Ti_3C_2T_x$/GCE sensor

Before modifying the glassy carbon electrode (GCE), the GCE was firstly polished using Al_2O_3 (0.05 μm) on the chamois leather for 5 min until appeared a bright mirror and rinsed repeatedly by ultrapure water for several times, and finally dried at room temperature. Then 20 μL of $Ti_3C_2T_x$ aqueous solution (5 mg mL^{-1}) mixed with ChOx solution (0.2 U μL^{-1}) together ultrasonic for 5 min. Following, 10 μL of Chit (6 mg mL^{-1}) solution was added to the above mixture solution followed by sonicating for 5 min. By now the $Ti_3C_2T_x$ shows negatively charged due to the abundance of –OH or –F groups, it could be well adhered in Chit solution, under the Coulomb effect, formed a uniform film on the surface of GCE (Shan et al., 2010). 5 μL of the suspension of Chit/ChOx/$Ti_3C_2T_x$ was slowly casted onto the surface of a freshly polished GCE. The modified electrode was dried at room temperature for further measurements.

3. Results and discussion

3.1. Structural characterization

The different morphology of the synthesized $Ti_3C_2T_x$ was investigated by SEM. As shown in Fig. 2A, the $Ti_3C_2T_x$ clearly showed an accordion-like structure resembled graphene. Each other sheets were separated and exfoliated multilayers less than 50 nm. At the same time, the synthesized $Ti_3C_2T_x$ has a large specific surface area, which is beneficial to immobilize the cholesterol oxidase. Furthermore, the $Ti_3C_2T_x$ was scanned over the 2θ range of 5 - 75° to identify the structure. From Fig. 2B, compared to Ti_3AlC_2, the Al layers were etched totally. In addition, some diffraction peaks (002), (004), and (006) peaks shifted to lower angles and tended to be broadened due to an enlarged interlayer spacing.

Fig. 2C showed the enzyme immobilization, the GCE surface formed a compact composite film. Interestingly, the 2D nanostructure of $Ti_3C_2T_x$ was beneficial to retaining the biological activity, embedding ChOx and promoting the transport of enzyme substances and products. The porous structure of the composite film Chit/ChOx/$Ti_3C_2T_x$ improved the effective specific surface area of the modified electrode, thus improved the performance of the fabricated biosensor.

As is known to all, FT-IR is the most effective means to research the structure of ChOx inset into the $Ti_3C_2T_x$ on the GCE. As seen in Fig. 2D, there are two strong peaks located at 3435 cm^{-1} (3379 cm^{-1}) and 1640 cm^{-1}, which may be the –OH or coordinated H_2O in the samples of $Ti_3C_2T_x$ and ChOx/$Ti_3C_2T_x$ nanocomposites. The amide (1600-1700 cm^{-1}) is corresponding to the –C═O stretching vibration of peptide chain in protein. The amide (1500-1620 cm^{-1}) is attributed to the combination of -N-H bending and C–N stretching (Lu et al., 2008). The absorption peaks at 1640 cm^{-1} and 1550 cm^{-1} are shown to agree with the characteristic absorption peaks of native cholesterol oxidase, which suggest the ChOx retain structure after forming ChOx/$Ti_3C_2T_x$ nanocomposites and prove the good biocompatibility of $Ti_3C_2T_x$.

3.2. CV and EIS characterization of $Ti_3C_2T_x$ modified electrodes

Cyclic voltammetry (CV) was performed with different modified electrodes immersed in 1 mM $Fe(CN)_6^{3-/4-}$ solution containing 0.1 M KCl and 1.0 mM cholesterol at a scan rate of 100 mV s^{-1} and the potential ranging from −1.0 V to 1.0 V (Fig. 3A). A pair of well-defined redox peaks were given at bare GCE (curve a). After GCE modified with ChOx/Chit, the redox peak current of $Fe(CN)_6^{3-/4-}$ significantly decreased (curve b). However, the CV current responses of ChOx/Chit/$Ti_3C_2T_x$ were enhanced significantly (curve c), especially in the remarkable increase of reduction peak current. This increased CV response most likely according to the sensitive electronic characteristics and strong adsorption capacity of $Ti_3C_2T_x$, was promoted by the intercalation capacity of $Ti_3C_2T_x$, which could give rise to a high load efficiency of cholesterol on the electrode surface.

It is also necessary to investigate the electron transfer properties of the different modified GCE through EIS. The frequency range from 0.1 kHz to 100 kHz. Open circuit voltage was 0.19 V. Alternating voltage was 5 mV. As shown in Fig. 3B, all of the EIS curves appear a typical semicircle or straight line in the high/low frequency scope. There is semicircular part at high frequencies corresponds to the electron transfer process, and diameter is equal to the electron transfer resistance (Rct). The diffusion process is linear part at lower frequencies. It is clear that $Ti_3C_2T_x$/GCE (b, Rct = 45.85 Ω) has very small semicircle diameter of EIS curve compared with bare GCE (c, Rct = 200.9 Ω), which is due to the excellent conductivity and favorable electron transfer kinetics of this sheetlike nanomaterial. When ChOx was modified with Chit onto bare GCE, the Rct increased from 200.9 Ω to 343.0 Ω indicating that the layer of ChOx and Chit have formed on the electrode. ChOx hinders the electron transport. After the $Ti_3C_2T_x$ was combined with Chit and ChOx

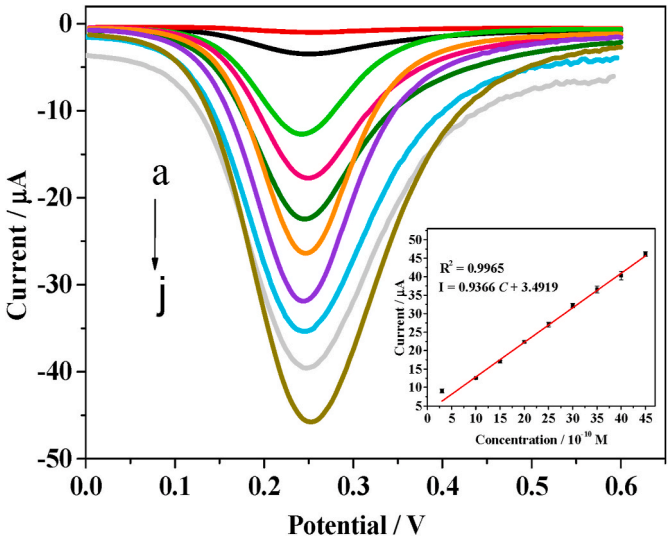

Fig. 4. DPV of the Chit/ChOx/$Ti_3C_2T_x$/GCE biosensor in different concentrations of cholesterol (a–j): 0, 0.3, 1, 1.5, 2.0, 2.5, 3.0, 3.5, 4.0, 4.5 nM, respectively, and 1 mM $Fe(CN)_6^{3-/4-}$ containing 0.1 M KCl. Inset is calibration plot of cholesterol.

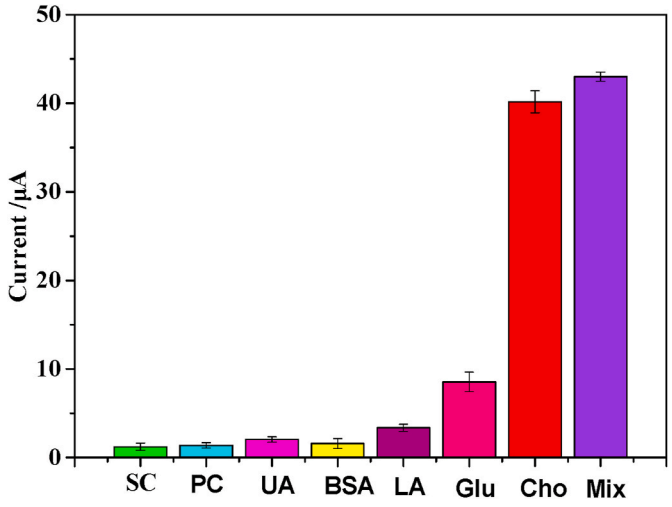

Fig. 5. The interference of various species in the detection of cholesterol.

to modify GCE electrode, the Rct decreased remarkably from 343.0 Ω to 118.7 Ω. The result indicates that $Ti_3C_2T_x$ speeds up the electron transfer on the surface of electrode, which increases the electrical conductivity. All of above match with the CV measurement results.

3.3. Optimization of experiment parameters

3.3.1. Optimization of scan rate

To explore the reaction kinetics, Chit/ChOx/$Ti_3C_2T_x$/GCE is studied by CV with different scanning rates at the potential ranging from −1.0 V to 1.0 V in the presence of cholesterol. As depicted in Fig. S1A, the redox peak current increased linearly when the scan rate increased from 20 mV s^{-1} to 200 mV s^{-1}. As shown in Fig. S1B, the linear regressions of anodic and cathodic peak current were I_a = 0.143 v + 13.209 (R^2 = 0.9956) and I_c = −0.617 v - 30.16 (R^2 = 0.9961), respectively. It indicates that the electrode reaction process is a surface adsorption controlled process rather than a diffusion controlled process. The possible reaction mechanism for electrochemical oxidation of cholesterol was shown in Fig. S2.

3.3.2. Optimization of the amount of $Ti_3C_2T_x$

To improve the sensitivity of the biosensor, the amount of $Ti_3C_2T_x$ was further investigated (Fig. S3A). DPV was applied to study electrochemical performance in 0.1 M PBS containing 1.0 mM cholesterol. As shown in Fig. S3A, with $Ti_3C_2T_x$ loading increasing from 1 mg mL^{-1} to 8 mg mL^{-1}, the current response appeared the maximum current response when $Ti_3C_2T_x$ reaches 5 mg mL^{-1}, subsequently, the current response decreased gradually. But excessive modified materials would lead to obstacles of electron transport. Thus, 5 mg mL^{-1} was selected as the optimum concentration.

3.3.3. Optimization of pH value of the substrate solution

Fig. S3B showed that the effect of pH value of PBS for the response of cholesterol at the electrochemical biosensor was investigated ranging from 5.0 to 8.0. When the pH value increased to more than 7.0, the current response of cholesterol decreased, which might be due to the potential inactivation of ChOx in overly alkaline PBS solutions. So the PBS solution (pH 7.0) was the optimal support electrolyte solution.

3.3.4. Optimization of the amount of ChOx

As shown in Fig. S4, with the concentration of ChOx ranging from 0.05 U μL^{-1} to 0.2 U μL^{-1}, the response current increased continuously. When the amount of ChOx continued to increase, the response current decreased significantly. It might be that the amount of ChOx was too much, which hindered electron transfer and reduced the response value of current. Excessive amount of ChOx would reduce the sensitivity of the biosensor and seriously affect the detection performance. Therefore, the optimal ChOx dosage was 0.2 U μL^{-1} in the following test.

3.4. Determination of cholesterol

Under optimal experimental conditions, at a scan rate of 100 mV s^{-1} and the potential ranging from 0 to 0.6 V, cholesterol was tested via DPV method. As shown in Fig. 4, the peak currents of cholesterol increased with the increase of cholesterol concentration, and there was a good linear relationship between the peak currents and the concentrations of cholesterol in the range of 0.3 – 4.5 nM. Corresponding linear regression equation was I (μA) = 0.9366 C × (10^{-10} M) + 3.4919 (R^2 = 0.9965). The LOD was calculated to be 0.11 nM (LOD = 3 × SD/S). SD is the standard deviation of the blank sample signal and S is the slope of the calibration curve. The sensitivity was 132.66 μA nM^{-1} cm^{-2}. The analytical performances of the biosensor in this study and other enzyme-based electrochemical sensors in recently reported literature for the detection of cholesterol were listed in Table S1. Obviously, the present work is suitable for placement among the enzymatic electrochemical cholesterol sensors reported with low detection limit and long linear range. The excellent performance of the biosensor was attributed to the synergistic effects between $Ti_3C_2T_x$ with large specific surface area and good conductivity. Moreover, a number of reactive functional groups in $Ti_3C_2T_x$ can favorably bind to functional groups of enzyme through covalent bonds or hydrogen bonds. ChOx remained intact on the electrode surface for long periods, which makes the biosensor stable.

3.5. Interference studies, stability, and reproducibility

To estimate the selectivity of the fabricated biosensor, there are potential interfering substances including sodium chloride (SC), potassium chloride (PC), urea acid (UA), bovine serum albumin (BSA), glucose (Glu), and lactic acid (LA) in the detection of cholesterol were investigated as shown in Fig. 5. It found that no significant interference was observed in the presence of these interferences with 4.5 nM cholesterol. And the current response in the mixed solution was almost the same as that in the detection of cholesterol. Therefore, the Chit/ChOx/$Ti_3C_2T_x$/GCE biosensor has a strong anti-interference ability.

In addition, the long-term stability of Chit/ChOx/$Ti_3C_2T_x$/GCE was assessed by monitoring 2 nM cholesterol applied for DPV measurements

Table 1
Determination of cholesterol in real samples by electrochemical.

Samples	Added (10^{-9} M)	Found (10^{-9} M)	RSD (%) (n = 5)	Recovery (%)
I	1.0	1.77	4.8	110.2
II	2.0	2.78	2.5	105.6
III	4.0	4.53	0.80	96.3

intermittently after storage at room temperature for 15 days. As shown in Fig. S5, the current response still maintained 98.2% of the initial value after 15 days. It indicated that the biosensor had excellent stability. Under the same experimental condition, the reproducibility was evaluated using five independent Chit/ChOx/$Ti_3C_2T_x$/GCE biosensors, which were used to determine 3 nM cholesterol. Fig. S6 suggested that the relative standard deviations (RSD) of these five individual sensors were less than 4.5%, which exhibited excellent reproducibility.

3.6. Real sample analysis

In order to further investigate the feasibility of the Chit/ChOx/$Ti_3C_2T_x$/GCE biosensor in practical sample analysis, the accuracy of the detection was evaluated by the method of spiked recovery (Table 1). The cholesterol content of human serum was diluted to 50-fold using PBS (0.1 M pH 7.0). It was determined to be 0.674 nM. Compared with the standard sample (0.674 nM) experiment, it was observed that the amount of cholesterol was found to be 0.713 nM (RSD = 1.47%, n = 5) using the fabricated biosensor.

It could be found from Table 1 that the recoveries obtained from the serum samples were 96.3%– 110.2%, meanwhile, the RSD were less than 4.8%. The results indicated this biosensor based on Chit/ChOx/$Ti_3C_2T_x$/GCE had excellent stability and repeatability. Hence, this biosensor can be implemented for the rapid and efficient detection of cholesterol in practical samples.

4. Conclusion

In summary, $Ti_3C_2T_x$ nanocomposites were prepared by etching Ti_3AlC_2 with HCl and LiF. The synthesized $Ti_3C_2T_x$ exhibited large specific area, biocompatibility, excellent electronic conductivity, and good dispersion in aqueous phase, which played an important part in electron transfer. Interestingly, the fabricated biosensor of immobilizing ChOx based on Chit/$Ti_3C_2T_x$ showed an outstanding performance for cholesterol with a low detection limit of 0.11 nM, and a high sensitivity of 132.66 μA nM^{-1} cm^{-2}. Furthermore, this biosensor was applied to rapid detection of cholesterol in real sample with good recoveries. Recently, in the face of the COVID-19 pandemic, biosensors have become particularly important in reducing disease transmission and facilitating medical treatment. At present, the biomedical applications of some Xenes (e.g., phosphorene) have been widely explored (Tao et al., 2019; Qiu et al., 2019). Some newly synthesized MXene nanomaterials are still at the beginning of their bio-applications, which means that in the near future these MXene will have broad application prospects. Finally, we firmly believe that the efficient development of MXene nanomaterials for the construction of advanced biosensors with high sensitivity and selectivity will be a great direction of medical care.

CRediT authorship contribution statement

Tianzi Xia: Investigation, Writing – original draft. **Guangyan Liu:** Data curation, review. **Junjie Wang:** Data curation. **Shili Hou:** Supervision, Writing – review & editing. **Shifeng Hou:** Writing – review & editing.

Declaration of competing interest

The authors declare that they have no known competing financial interests or personal relationships that could have appeared to influence the work reported in this paper.

Acknowledgements

The authors acknowledge was supported by Guangxi science and technology base and talent special project (No. AD19110093), Guangxi Basic Ability Improvement Project for Young and Middle-aged University Teachers (No. 2019KY0274), and Foundation of Guilin University of Technology (No. GLUT2017132).

Appendix A. Supplementary data

Supplementary data to this article can be found online at https://doi.org/10.1016/j.bios.2021.113243.

References

Alwarappan, S., Joshi, R.K., Ram, M.K., Kumar, A., 2010a. Appl. Phys. Lett. 96, 263702. https://doi.org/10.1063/1.3458698.
Alwarappan, S., Liu, C., Kumar, A., Li, C.Z., 2010b. J. Phys. Chem. C 114, 12920–12924. https://doi.org/10.1021/jp103273z.
Alwarappan, S., Boyapalle, S., Kumar, A., Li, C.Z., Mohapatra, A., 2012. J. Phys. Chem. C 116, 6556–6559. https://doi.org/10.1021/jp211201b.
Amiri, M., Arshi, S., 2020. Electroanalysis 32, 1391–1407. https://doi.org/10.1002/elan.201900669.
Chitra, J., Ghosh, M., Mishra, H.N., 2017. Food Contr. 78, 342–349. https://doi.org/10.1016/j.foodcont.2016.10.008.
Devadoss, A., Burgess, J.D., 2004. J. Am. Chem. Soc. 126, 10214–10215. https://doi.org/10.1021/ja047856e.
Farshchi, F., Hasanzadeh, M., Feyziazar, M., Saadati, A., Hassanpour, S., 2020. Anal. Methods 12, 1212–1217. https://doi.org/10.1039/C9AY02789K.
Huang, S., Yang, E., Yao, J., Chu, X., Liu, Y., Zhang, Y., Xiao, Q., 2019. ACS Omega 4, 9333–9342. https://doi.org/10.1021/acsomega.9b00874.
Huo, X., Liu, X., Liu, J., Sukumaran, P., Alwarappan, S., Wong, D.K.Y., 2016. Electroanalysis 28, 1730–1749. https://doi.org/10.1002/elan.201600166.
Kalambate, P.K., Gadhari, N.S., Li, X., Rao, Z., Navale, S.T., Shen, Y., Patil, V.R., Huang, Y., 2019. TrAC Trends Anal. Chem. (Reference Ed.) 120, 115643. https://doi.org/10.1016/j.trac.2019.115643.
Liu, H., Duan, C., Yang, C., Shen, W., Wang, F., Zhu, Z., 2015. Sens. Actuators, B 218, 60–66. https://doi.org/10.1016/j.snb.2015.04.090.
Liu, J., Jiang, X., Zhang, R., Zhang, Y., Wu, L., Lu, W., Li, J., Li, Y., Zhang, H., 2019. Adv. Funct. Mater. 29, 1807326. https://doi.org/10.1002/adfm.201807326.
Lu, X., Zhou, J., Lu, W., Liu, Q., Li, J., 2008. Biosens. Bioelectron. 23, 1236–1243. https://doi.org/10.1016/j.bios.2007.11.006.
Ma, X., Tu, X., Gao, F., Xie, Y., Huang, X., Fernandez, C., Qu, F., Liu, G., Lu, L., Yu, Y., 2020. Sens. Actuators, B 309, 127815. https://doi.org/10.1016/j.snb.2020.127815.
Maduraiveeran, G., Sasidharan, M., Ganesan, V., 2018. Biosens. Bioelectron. 103, 113–129. https://doi.org/10.1016/j.bios.2017.12.031.
Malig, J., Romero-Nieto, C., Jux, N., 2012. Adv. Mater. 24, 800–805. https://doi.org/10.1002/adma.201103697.
Naguib, M., Kurtoglu, M., Presser, V., Lu, J., Niu, J., Heon, M., Hultman, L., Gogotsi, Y., Barsoum, M.W., 2011. Adv. Mater. 23, 4248–4253. https://doi.org/10.1002/adma.201102306.
Nandini, S., Nalini, S., Reddy, M.B.M., Suresh, G.S., Melo, J.S., Niranjana, P., Sanetuntikul, J., Shanmugam, S., 2016. Bioelectrochemistry 110, 79–90. https://doi.org/10.1016/j.bioelechem.2016.03.006.
Narwal, V., Deswal, R., Batra, B., Kalra, V., Hooda, R., Sharma, M., Rana, J.S., 2019. Steroids 143, 7–17. https://doi.org/10.1016/j.steroids.2018.12.003.
Qiu, M., Singh, A., Wang, D., Qu, J., Swihart, M., Zhang, H., Prasad, P.N., 2019. Nano Today 25, 135–155. https://doi.org/10.1016/j.nantod.2019.02.012.
Sajid, M., 2021. Anal. Chim. Acta 1143, 267–280. https://doi.org/10.1016/j.aca.2020.08.063.
Seh, Z.W., Fredrickson, K.D., Anasori, B., Kibsgaard, J., Strickler, A.L., Lukatskaya, M.R., Gogotsi, Y., Jaramillo, T.F., Vojvodic, A., 2016. ACS Energy Lett 1, 589–594. https://doi.org/10.1021/acsenergylett.6b00247.
Sekretaryova, A.N., Beni, V., Eriksson, M., Karyakin, A.A., Turner, A.P.F., Vagin, M.Y., 2014. Anal. Chem. 86, 9540–9547. https://doi.org/10.1021/ac501699p.
Shan, C., Yang, H., Han, D., Zhang, Q., Ivaska, A., Niu, Li, 2010. Biosens. Bioelectron. 25, 1070–1074. https://doi.org/10.1016/j.bios.2009.09.024.
Sinha, A., Basiruddin, S.K., Chakraborty, A., Jana, N.R., 2015. ACS Appl. Mater. Interfaces 7, 1340–1347. https://doi.org/10.1021/am507817b.
Soomro, R.A., Jawaid, S., Zhu, Q., Abbas, Z., Xu, B., 2020. Chin. Chem. Lett. 31, 922–930. https://doi.org/10.1016/j.cclet.2019.12.005.
Sun, Q., Fang, S., Fang, Y., Qian, Z., Feng, H., 2017. Talanta 167, 513–519. https://doi.org/10.1016/j.talanta.2017.02.060.

Tao, W., Kong, N., Ji, X., Zhang, Y., Sharma, A., Ouyang, J., Qi, B., Wang, J., Xie, N., Kang, C., Zhang, H., Farokhzad, O., Kim, J.S., 2019. Chem. Soc. Rev. 48, 2891–2912. https://doi.org/10.1039/c8cs00823j.

Urbankowski, P., Anasori, B., Hantanasirisakul, K., Yang, L., Zhang, L., Haines, B., May, S.J., Billinge, S.J.L., Gogotsi, Y., 2017. Nanoscale 9, 17722–17730. https://doi.org/10.1039/C7NR06721F.

Wan, P., Wen, X., Sun, C., Chandran, B.K., Zhang, H., Sun, X., Chen, X., 2015. Small 11, 5409–5415. https://doi.org/10.1002/smll.201501772.

Wang, F., Yang, C., Duan, M., Tang, Y., Zhu, J., 2015. Biosens. Bioelectron. 74, 1022–1028. https://doi.org/10.1016/j.bios.2015.08.004.

Wu, L., Lu, X., Dhanjai Wu, Z.S., Dong, Y., Wang, X., Zheng, S., Chen, J., 2018. Biosens. Bioelectron. 107, 69–75. https://doi.org/10.1016/j.bios.2018.02.021.

Wu, X., Chai, Y., Yuan, R., Zhong, X., Zhang, J., 2014. Electrochim. Acta 129, 441–449. https://doi.org/10.1016/j.electacta.2014.02.103.

Yang, S., Liu, Y., Chen, W., Jin, W., Zhou, J., Zhang, H., Zakharova, G.S., 2016. Sens. Actuators, B 226, 478–485. https://doi.org/10.1016/j.snb.2015.12.005.

Yao, C., Zhang, W., Xu, L., Cheng, M., Su, Y., Xue, J., Liu, J., Hou, S., 2021. Separ. Purif. Technol. 263, 118365. https://doi.org/10.1016/j.seppur.2021.118365.

Yu, L., Hu, L., Anasori, B., Liu, Y.T., Zhu, Q., Zhang, P., Gogotsi, Y., Xu, B., 2018. ACS Energy Lett 3, 1597–1603. https://doi.org/10.1021/acsenergylett.8b00718.

Yuan, C., 2013. Talanta 109, 167–172. https://doi.org/10.1016/j.talanta.2013.02.002.

Zandi, A., Gilani, A., Abbasvandi, F., Katebi, P., Tafti, S.R., Assadi, S., Moghtaderi, H., Parizi, M.S., Saghafi, M., Khayamian, M.A., Davari sh, Z., Hoseinpour, P., Gity, M., Sanati, H., Abdolahad, M., 2019. Biosens. Bioelectron. 142, 111566. https://doi.org/10.1016/j.bios.2019.111566.

Zhang, P., Zhu, Q., Guan, Z., Zhao, Q., Sun, N., Xu, B., 2020. Chemsuschem 13, 1621–1628. https://doi.org/10.1002/cssc.201901497.

Zhao, M., Li, Y., Ma, X., Xia, M., Zhang, Y., 2019. Talanta 200 293–299. https://doi.org/10.1016/j.talanta.2019.03.060.